Title

An Activity-Based Nanosensor for Traumatic Brain Injury.

Journal

ACS Sensors, 5(3)

Authors

Kudryashev, Julia

Waggoner, Lauren

Leng, Hope

et al.

Publication Date

2020-03-27

DOI

10.1021/acssensors.9b01812

Peer reviewed

Published in final edited form as:

ACS Sens. 2020 March 27; 5(3): 686–692. doi:10.1021/acssensors.9b01812.

An Activity-Based Nanosensor for Traumatic Brain Injury

Julia A. Kudryashev[1], **Lauren E. Waggoner**[2], **Hope T. Leng**[1], **Nicholas H. Mininni**[1], **Ester J. Kwon**[1,*]

[1]Department of Bioengineering, University of California, San Diego, La Jolla, California 92093, United States

[2]Department of Nanoengineering, University of California, San Diego, La Jolla, California 92093, United States

Abstract

Currently, traumatic brain injury (TBI) is detected by medical imaging; however, medical imaging requires expensive capital equipment, is time- and resource-intensive, and is poor at predicting patient prognosis. To date, direct measurement of elevated protease activity has yet to be utilized in order to detect TBI. In this work, we engineered an activity-based nanosensor for TBI (TBI-ABN) that responds to increased protease activity initiated after brain injury. We establish that a calcium-sensitive protease, calpain-1, is active in the injured brain hours within injury. We then optimize the molecular weight of a nanoscale polymeric carrier to infiltrate into injured brain tissue with minimal renal filtration. A calpain-1 substrate that generates fluorescent signal upon cleavage was attached to this nanoscale polymeric carrier to generate an engineered TBI-ABN. When applied intravenously to a mouse model of TBI, our engineered sensor is observed to locally activate in the injured brain tissue. This TBI-ABN is the first demonstration of a sensor that responds to protease activity to detect TBI.

Keywords

Traumatic brain injury; activity-based nanosensor; nanomedicine; calpain-1; protease activity

Traumatic brain injury (TBI) affects over 2.8 million people annually in the United States and leads to the hospitalization of ~300,000 patients per year.[1] Among TBI patients who require surgical intervention, there is a 50% lower mortality rate and decreased length of stay if they receive surgery within 4 hours of hospital admission,[2] indicating the importance of rapid diagnosis and triage to improve outcomes. However, current diagnosis is achieved by medical imaging, typically computed tomography (CT) and magnetic resonance imaging

*Corresponding Author, ejkwon@ucsd.edu.

Author Contributions

J.A.K. and E.J.K.: project conceptualization, experimental design, data acquisition and analysis, manuscript preparation; L.E.W.: experimental design, data acquisition; H.T.L. and N.H.M.: data acquisition. All authors have given approval to the final version of the manuscript.

Supporting Information. Calpain-1 distribution in brain slices; traced organs for biodistribution; kinetics conjugation control; sensor signal in uninjured hemispheres; sensor localization in areas of extravasation. This material is available free of charge via the Internet at http://pubs.acs.org.

The authors declare no competing financial interest.

(MRI), both of which are time- and resource-intensive and have a limited ability to predict patient prognosis.[3] Moreover, while medical imaging can identify macroscopic structural deformations in the brain, it currently does not yield information on the destructive biological activity that may unfold after injury This secondary injury, which may include sustained protease activity, inflammation, excitotoxicity, and neuronal death, begins immediately after the primary injury and may lead to chronic neurodegeneration and a poorer patient prognosis.[4] Thus, a diagnostic that yields information on biological activity may inform improved clinical care.

Breakdown products shed into the blood and cerebrospinal fluid have been recently investigated as biomarkers to detect pathological processes in TBI.[5] These breakdown products originate from the degradation of nervous tissue as part of a prolonged secondary injury that begins within minutes after TBI.[6] To date there is only one TBI biomarker-based diagnostic on the market; it is based on two separate ELISAs to measure serum levels of the breakdown products GFAP and UCH-L1.[7] However, measurement of these biomarkers relies on the generation, stability, and transport of these byproducts;[8] direct measurement of degradative activity may be more representative of disease and therefore provide information that is more actionable for intervention. Calpain-1, a calcium-dependent protease expressed in neurons, glia, and endothelial cells within the brain, undergoes sustained activation after TBI due to pathological elevations of intracellular calcium.[6,9,10] Calpain-1 activity generates many breakdown products that are currently under investigation as biomarkers for TBI, including myelin basic protein, neurofilaments, and αII-spectrin.[5] Calpain-1 inhibition has been under investigation as a treatment for TBI,[11] and its byproducts can potentially predict patient prognosis after mild and severe TBI,[12,13] highlighting the importance of calpain-1 in the injury sequelae and its prognostic potential. Thus, the detection of calpain-1 protease activity is a promising candidate for TBI diagnosis.

To explore the potential of activity-based sensors to detect TBI, our goal was to engineer a vascularly-administered sensor that can accumulate in injured brain tissue and produce a signal in response to calpain-1 activity (Figure 1A). A similar activity-based sensor strategy has been demonstrated for the sensitive detection of cancer and liver fibrosis in previous work,[14,15] but has yet to be applied to any brain disorders. First, we established increased calpain-1 activity that is independent of calpain-1 expression levels in the first few hours after TBI in mice, validating the need for a sensor of enzyme activity rather than enzyme levels. In order to engineer a diagnostic that can be delivered into the vasculature, we exploit size-dependent accumulation of nanoscale polymeric carriers into the site of injury, where the blood brain barrier (BBB) is compromised and allows extravasation of nanoscale materials. To detect calpain-1 activity, we engineered a FRET peptide which activates in the presence of active calpain-1. Combining the peptide and carrier, we engineered a TBI activity-based nanosensor, TBI-ABN. This TBI-ABN activates at the site of injury in a mouse model of brain injury after intravenous administration. To our knowledge, TBI-ABN is the first demonstration of an activity-based sensor for TBI.

Experimental Section

Synthesis of PEG Conjugates.

Calpain substrate peptide (QSY21-QEVYGAMP-K(Cy5)-PEG2-GC-NH2) was synthesized by CPC Scientific Inc. (Sunnyvale, CA, USA). PEG2 is polyethylene glycol. 8-arm PEG amine and PEG maleimide (tripentae-rythritol) were purchased from Jenkem Technology (Beijing, China). PEG amine was reacted with 1 mole equivalent of VivoTag-S 750 (PerkinElmer, Boston, MA, USA). PEG maleimide was reacted with 1, 2, and 4 mole equivalences of peptide in the presence of 50 mM triethylamine (TEA) and quenched with an excess of cysteine. All conjugates were dialyzed into water, and final concentrations were determined by absorbance of VivoTag or Cy5 using a Spark Multimode Microplate Reader (Tecan Trading AG, Switzerland). The L-cysteine PEG maleimide control was dissolved by weight. Hydrodynamic diameters of unconjugated PEG amine were measured via DLS with a Zetasizer Nano (Malvern Panalytical).

In vitro reaction kinetics assay.

Free peptide and conjugates were incubated with 26.6 nM recombinant human calpain-1 (Sigma-Aldrich) in 50 mM HEPES, 50 mM NaCl, 2 mM EDTA, 5 mM CaCl2, 5 mM beta-mercaptoethanol, 10% mouse plasma in PBS, or 13.5 nM human alpha-thrombin (Haematologic Technologies) in TCNB buffer. Mouse plasma was prepared by centrifuging blood collected with EDTA. Fluorescence readings were taken every 90 seconds at 37 °C for 1 hour. Reaction curves were normalized to controls, and their initial velocities were fitted to a Michaelis-Menten curve in GraphPad Prism (8.1.2).

Controlled cortical impact (CCI) mouse model of TBI.

All mouse protocols were approved by the University of California San Diego's Institutional Animal Care and Use Committee (IACUC). 8–12 week old female C57BL/6J mice (Jackson Labs) were used for all experiments. Mice were anesthetized with 2.5% isoflurane and the head was secured in a stereotaxic frame. A midline incision was made to expose the skull, and a 4 mm diameter craniotomy was performed over the right hemisphere between bregma and lambda. The controlled cortical impact was applied to the exposed dura of the cortex with the ImpactOne (Leica Biosystems) fitted with a stainless steel 2 mm diameter probe at a velocity of 3 m/s and a 2 mm depth.

Biodistribution and in vivo sensor activation.

2 hours after CCI, 2 nmoles of VivoTag-PEG in 100 μL PBS (n=4 each for biodistribution) or 8 nmoles of TBI-ABN in 100 μL PBS (n=6 for sensor activation analysis) were intravenously administered via the tail-vein. Control mice received the same volume of PBS. 2 hours after administration, mice were trans-cardially perfused with USP saline followed by 10% formalin. Fluorescence was measured with an Odyssey scanner (Li-Cor Biosciences) on the same day as collection. Mean fluorescence intensity per area was analyzed using ImageJ.

Immunohistochemistry and sensor quantification in brain tissue slices.

Organs were fixed with 10% formalin solution at 4 °C overnight, equilibrated in 30% w/v sucrose, and frozen in OCT (Tis-sue-Tek). 10 μm thick coronal tissue slices were stained using conventional protocols. The following primary antibodies were used: 1:200 calpain-1 (Abcam, ab108400), and 1:200 CD31 (BD, 553370). Sensor activation was quantified in 3 tissue slices per brain up to 1.5 mm caudal from the center of injury. Cy5 signal in each slice extending 1.5 mm down from the top of the cortex was averaged between slices from each brain then normalized to the signal from uninjured PBS controls using ImageJ. Images were captured with a Nikon Eclipse Ti2 microscope fitted with a Hamamatsu Orca-Flash 4.0 digital camera.

Protein analysis.

At the designated time points after injury, injured and contralateral cortices were harvested and immediately frozen. Sham injured mice received a craniotomy and no injury and tissue was harvested 3 hours after surgery. Western blots were performed following conventional protocols. The following primary antibodies were used: 1:2000 αII-spectrin (Abcam, ab11755), 1:1000 calpain-1 (Abcam, ab108400), or 1:5000 α-tubulin (Cell Signaling, 3873). Membranes were imaged on a Li-Cor Odyssey scanner and densitometric analysis of the western blots was done in ImageJ.

Software and Statistics.

All data was analyzed in GraphPad Prism (8.1.2). All post-hoc tests were conducted with $p<0.05$ to identify statistical significance between samples. All images were analyzed with ImageJ (1.52p).

Results and Discussion

Calpain-1 locally activates in a mouse model of TBI

We first established the levels of calpain-1 activity and protein levels in a mouse model of TBI. The controlled cortical impact (CCI) model of TBI is a reproducible and well-characterized method to create a localized injury in the brain.[16–18] To assess calpain-1 activity, 150 kDa and 145 kDa breakdown products of the native calpain-1 substrate αII-spectrin were measured, as described previously.[19] These spectrin breakdown products (SBDP) were shown to increase to greater than 10-fold in the injured hemisphere at 3 hours post injury compared to uninjured brains (Figure 1B, C). This increase was sustained up to 96 hours post injury. By contrast, the uninjured, contralateral hemisphere did not show significant elevation of SBDPs. A sham control group that underwent a craniotomy but no injury exhibited similar levels of SBDPs to uninjured mice, confirming that spectrin proteolysis was the result of direct impact to the brain tissue and not the surgical procedures. We thus establish that calpain-1 activity is increased after CCI and activity is localized to the injured hemisphere, consistent with previously reported rodent models of CCI.[17,19–21]

To determine that increased spectrin cleavage was due to increased activity of calpain-1 and not increased levels of calpain-1, calpain-1 protein levels were also measured. No significant changes were observed in the protein levels of the 80 kDa large subunit of calpain-1 between

injured and uninjured brains (Figure 1D, E). Furthermore, assessment of calpain-1 via immunohistochemistry of brain slices showed only a local increase in calpain-1 detected 4 hours post-injury in the immediate injury area, whereas calpain-1 levels appeared to be unchanged in the uninjured cortex and the greater injury periphery when compared to uninjured brains (Figure S1). These results indicate that the observed increase in αII-spectrin proteolysis (Figure 1B) is likely due to increased calpain-1 activity and not increased calpain-1 expression. Previous studies have shown that calpain-1 expression can be increased after injury, but its elevation is delayed by ~24 hours.[22] Therefore a sensor to detect calpain-1 activity may be effective in the first few hours after TBI.

Large molecular weight polymeric carriers accumulate in the site of injury after CCI.

We next focused on a nanoscale delivery carrier for our nanosensor. Shortly after TBI, the vasculature at the site of injury is compromised due to the mechanical damage followed by dysregulation of the neurovascular unit.[23,24] This pathological hallmark of TBI allows for the delivery of nanoscale cargo to the brain within the first 24 hours after injury, similar to the enhanced permeability and retention (EPR) effect described for nanoparticles in tumors.[25] On their own, small peptides have a short circulation half-life in vivo due to renal clearance and proteolytic degradation in the bloodstream. We hypothesized that blood circulation time and subsequent tissue retention of the peptide would increase through its conjugation to a larger, neutrally-charged, and minimally immunogenic polymeric carrier such as polyethylene glycol (PEG).[26] While studies have been done on the biodistribution of rigid nanoparticles, including PEGylated polystyrene nanoparticles and liposomes after TBI,[27,28] and polystyrene nanoparticles after microdialysis probe insertion,[29] there has not yet been a study into the distribution of PEG after TBI. To maximize the delivery of the TBI nanosensor through the compromised BBB after injury, we evaluated how the molecular weight of 8-arm PEG affects its accumulation into the injured tissue after CCI injury. 8-arm PEG was chosen as the carrier because it allows for the possibility of multiplexing through conjugation of ligands to each individual arm. 10 kDa, 20 kDa, and 40 kDa PEG carriers were evaluated for distribution into major organs after intravenous injection 2 hours after CCI in mice (Figure 2A, S2). This timeline was chosen to be within the initial 4 hours of secondary injury after CCI when a quick diagnosis and intervention of calpain is critical.[17] The highest accumulation for 10 kDa PEG was seen in the kidneys with little accumulation in the brain, whereas the 20 kDa and 40 kDa PEG had significant accumulation in the injured brain and significantly less accumulation in the kidneys compared to the 10kDa PEG. In the brain, 20kDa and 40kDa PEG accumulated significantly more in the injured hemisphere than in the contralateral hemisphere by approximately 7-fold and 5-fold respectively (Figure 2B). The hydrodynamic radius of each carrier in PBS was measured to be 5.57 nm, 7.89 nm, and 10.25 nm for 10 kDa, 20 kDa, and 40 kDa PEG, respectively (Figure 2C). 10 kDa PEG is near the ~5 nm limit for renal filtration,[30,31] which is reflected in its significant accumulation into the kidneys compared to the 20 and 40 kDa sizes. All three carriers are smaller than the 500 nm size range of materials which have been observed to extravasate into injured tissue following TBI.[28,32] Thus, 8-arm PEG polymer carriers greater than 20kDa in size can accumulate in the injured brain.

Calpain substrate responds to calpain-1 activity.

To detect calpain-1 activity, we synthesized a calpain-1-responsive peptide comprised of the FRET pair Cy5 and QSY21 separated by a calpain-1-specific cleavage sequence (QEVYGAMP) taken from the native mouse αII-spectrin sequence (Figure 3A).[33] To measure kinetics of cleavage by calpain-1, several concentrations of peptide were incubated with recombinant calpain-1 enzyme in vitro and peptide cleavage was measured by dequenched Cy5 fluorescence (Figure 3B). Because blood cleavage is a major concern for a sensor administered intravenously, non-specific cleavage of our peptide by blood components was examined by incubation with mouse plasma or human alpha-thrombin. No significant cleavage of our substrate was observed (Figure 3C). This peptide was then conjugated to 40 kDa 8-arm PEG in order to increase its circulation time and retention in injured brain tissue when applied in vivo (Figure 2). 40 kDa PEG was used over 20 kDa PEG in order to increase solubility of the peptide, as precipitates were observed with 20 kDa conjugates. Multiple ratios of peptide:PEG were assessed via the same in vitro kinetics assay to optimize for sensor signal in response to calpain-1. It was observed that the conjugation of peptide:PEG in a 1:1 stoichiometric ratio led to a decrease in fluorescent signal (Figure 3B) as well as maximum cleavage velocity (Figure 3D) compared to free peptide. For example, the maximum cleavage velocity of peptide at an 8 μM concentration decreased from 1677.5 RFU/min to 692.1 RFU/min with conjugation. This decrease was not observed with peptide in the presence of free unconjugated PEG (Figure S3), suggesting that the direct conjugation of the peptide to PEG impacts peptide cleavage by calpain-1. The addition of multiple peptides:PEG in 2:1 and 4:1 conjugates led to further decreased cleavage velocities compared to 1:1 conjugate or free peptide (Figure 3D). Conjugates of 8:1 peptide:PEG precipitated out of solution, suggesting that the increased local concentration of peptides created by physical linkage to a polymeric carrier leads to a decrease in solubility. Due to the benefits of brain accumulation afforded by the PEG, a 1:1 stoichiometric ratio of peptide and PEG carrier was further evaluated in animal models of TBI.

TBI-ABN activates in injured brain tissue after CCI.

Finally, we tested the activation of the TBI nanosensor in a mouse model of TBI. We have established that calpain-1 has increased activity independent of expression after brain injury, greater than 20 kDa molecular weight PEG can accumulate in the injury site, and a FRET peptide substrate is cleaved by calpain-1. Extracellular release of calpain-1 and its substrates by necrotic neurons after injury has been observed in previous studies;[5,34] we therefore expect activation of our nanosensor without the need for cell internalization. Increased calpain-1 activity and intravenous access to the brain both occur within the same 4-hour time scale post-injury, so we expect that our TBI-ABN can localize and activate in the injured brain. We note that diagnosis of TBI within this 4-hour window has been demonstrated to be crucial to decrease patient morbidity.[2]

Mice were intravenously injected with sensor 2 hours after CCI injury and evaluated for sensor activation 2 hours after injection. In the first hours after CCI, focal neurodegeneration has been previously been shown to extend from the injury site down to the hippocampus;[17] based on these observations, the top 1.5 mm of coronal brain slices were analyzed for sensor activation after fluorescent imaging. The sensor showed significant activation in the injured

brain hemisphere with a higher activated sensor signal compared to background signal from both injured and uninjured brains (Figure 4A–C). There was minimal activation of the sensor in uninjured brains, likely due to unchanged calpain-1 activity (Figure 1B) and intact BBB. Additionally, there was little difference in signal in uninjured brains and the contralateral hemisphere of injured brains (Figure 4D, S4). These results provide evidence that the sensor produces a signal in response to injury.

We additionally investigated cellular distribution of sensor activation. Since the TBI-ABN was delivered through an intravenous injection, we assessed TBI-ABN activation in relation to the vasculature by staining for calpain-1 and the endothelial marker, CD31. In the injury periphery, activated TBI-ABN signal was found in proximity to calpain-1 and some signal was also positively stained for endothelial cells (Figure 4E,F). Signal was also detected in the hippocampal CA1 region and dentate gyrus (Figure S5), regions which are identified as sites of extravasation and neurodegeneration following CCI.[18,24] Neurons, glia, and endothelial cells populating these regions are known to experience calcium influxes and abnormal calpain activation following injury,[6,9] and are therefore potential sources for TBI-ABN signal.

Conclusions

We engineered a TBI activity-based nanosensor, TBI-ABN, which responds to calpain-1 activity, accumulates in injured brain tissue, and activates in a mouse model of brain injury. To our knowledge, our engineered TBI-ABN is the first sensor to detect enzyme activity in TBI and is a proof-of-concept for the development of future activity-based diagnostics for TBI. Activity-based sensors are gaining significance for their ability to be engineered in response to specific biological stimuli, allowing for the capture of pathological processes that cannot be detected by conventional molecular quantification methods.[35] There are notable examples of activity-based sensors in cancer: fluorescently activated polymers can identify tumor margins during surgical resection[36,37] and urinary sensors can detect and stratify tumors.[14,15,38] Based on these advances in cancer, measuring protease activity with an activity-based sensor to diagnose TBI is a promising strategy.

Now that we have established that a vascularly-delivered sensor can activate in brain injury in response to protease activity, in future work the TBI-ABN will be engineered to release biomarkers for minimally-invasive blood-based detection. Signal specificity can be increased by multiplexing substrates for the detection of proteases such as MMP-9, which has local increases in activity following TBI and contributes to BBB breakdown.[39] To further enhance sensitivity and increase tissue accumulation and retention, we can add active targeting ligands, for example peptides that bind extracellular matrix components exposed after injury.[40–42] In the long-term, TBI-ABN can be paired with inhibitors of protease activity, such as small molecule inhibitors of calpain-1[11] to create nanotheranostics that can detect and treat TBI.

Supplementary Material

Refer to Web version on PubMed Central for supplementary material.

Funding Sources

JAK is supported by the National Science Foundation (NSF) Graduate Research Fellowship Program under Grant No. DGE-1650112. Any opinions, findings, and conclusions or recommendations expressed in this material are those of the authors and do not necessarily reflect the views of the NSF.

ABBREVIATIONS

ABN	activity-based nanosensor
BBB	blood-brain barrier
CCI	controlled cortical impact
DLS	dynamic light scattering
TBI	traumatic brain injury

REFERENCES

(1). CDC. Surveillance Report of Traumatic Brain Injury-Related Emergency Department Visits, Hospitalizations, and Deaths—United States, 2014; 2019.

(2). Kim YJ The Impact of Time from ED Arrival to Surgery on Mortality and Hospital Length of Stay in Patients With Traumatic Brain Injury. J. Emerg. Nurs 2011, 37, 328–333. DOI: 10.1016/j.jen.2010.04.017. [PubMed: 21741566]

(3). Hofman PAM; Stapert SZ; van Kroonenburgh MJPG; Jolles J; de Kruijk J; Wilmink JT MR Imaging, Single-Photon Emission CT, and Neurocognitive Performance after Mild Traumatic Brain Injury. Am. J. Neuroradiol 2001, 22, 441–449. [PubMed: 11237964]

(4). Maas AIR; Stocchetti N; Bullock R Moderate and Severe Traumatic Brain Injury in Adults. Lancet Neurol. 2008, 7, 728–741. DOI: 10.1016/S1474-4422(08)70164-9. [PubMed: 18635021]

(5). Wang KK; Yang Z; Zhu T; Shi Y; Rubenstein R; Tyndall JA; Manley GT An Update on Diagnostic and Prognostic Biomarkers for Traumatic Brain Injury. Expert Rev. Mol. Diagn 2018, 18, 165–180. DOI: 10.1080/14737159.2018.1428089. [PubMed: 29338452]

(6). Andriessen TMJC; Jacobs B; Vos PE Clinical Characteristics and Pathophysiological Mechanisms of Focal and Diffuse Traumatic Brain Injury. J. Cell. Mol. Med 2010, 14, 2381–2392. DOI: 10.1111/j.1582-4934.2010.01164.x. [PubMed: 20738443]

(7). Bazarian JJ; Biberthaler P; Welch RD; Lewis LM; Barzo P; Bogner-Flatz V; Gunnar Brolinson P; Büki A; Chen JY; Christenson RH; et al. Serum GFAP and UCH-L1 for Prediction of Absence of Intracranial Injuries on Head CT (ALERT-TBI): A Multicentre Observational Study. Lancet Neurol. 2018, 17, 782–789. DOI: 10.1016/S1474-4422(18)30231-X. [PubMed: 30054151]

(8). Hori SS; Gambhir SS Mathematical Model Identifies Blood Biomarker-Based Early Cancer Detection Strategies and Limitations. Sci. Transl. Med 2011, 3, 109ra116 DOI: 10.1126/scitranslmed.3003110.

(9). Czogalla A; Sikorski AF Spectrin and Calpain: A “target” and a “Sniper” in the Pathology of Neuronal Cells. Cell. Mol. Life Sci 2005, 62, 1913–1924. DOI: 10.1007/s00018-005-5097-0. [PubMed: 15990959]

(10). Hamakubo T; Kannagi R; Murachi T; Matus A Distribution of Calpains I and II in Rat Brain. J. Neurosci 1986, 6, 3103–3111. DOI: 10.1523/JNEUROSCI.06-11-03103.1986. [PubMed: 3021924]

(11). Saatman KE; Creed J; Raghupathi R Calpain as a Therapeutic Target in Traumatic Brain Injury. Neurotherapeutics 2010, 7, 31–42. DOI: 10.1016/j.nurt.2009.11.002. [PubMed: 20129495]

(12). Siman R; Giovannone N; Hanten G; Wilde EA; McCauley SR; Hunter JV; Li X; Levin HS; Smith DH Evidence That the Blood Biomarker SNTF Predicts Brain Imaging Changes and Persistent Cognitive Dysfunction in Mild TBI Patients. Front. Neurol 2013, 4, 190 DOI: 10.3389/fneur.2013.00190. [PubMed: 24302918]

(13). Gan ZS; Stein SC; Swanson R; Guan S; Garcia L; Mehta D; Smith DH Blood Biomarkers for Traumatic Brain Injury: A Quantitative Assessment of Diagnostic and Prognostic Accuracy. Front. Neurol 2019, 10, 446 DOI: 10.3389/fneur.2019.00446. [PubMed: 31105646]

(14). Kwong GA; von Maltzahn G; Murugappan G; Abudayyeh O; Mo S; Papayannopoulos IA; Sverdlov DY; Liu SB; Warren AD; Popov Y; et al. Mass-Encoded Synthetic Biomarkers for Multiplexed Urinary Monitoring of Disease. Nat. Biotechnol 2013, 31, 63–70. DOI: 10.1038/nbt.2464. [PubMed: 23242163]

(15). Kwon EJ; Dudani JS; Bhatia SN Ultrasensitive Tumour-Penetrating Nanosensors of Protease Activity. Nat. Biomed. Eng 2017, 1, 0054 DOI: 10.1038/s41551-017-0054. [PubMed: 28970963]

(16). Xiong Y; Mahmood A; Chopp M Animal Models of Traumatic Brain Injury. Nat. Rev. Neurosci 2013, 14, 128–142. DOI: 10.1038/nrn3407. [PubMed: 23329160]

(17). Hall ED; Sullivan PG; Gibson TR; Pavel KM; Thompson BM; Scheff SW Spatial and Temporal Characteristics of Neurodegeneration after Controlled Cortical Impact in Mice: More than a Focal Brain Injury. J. Neurotrauma 2005, 22, 252–265. DOI: 10.1089/neu.2005.22.252. [PubMed: 15716631]

(18). Chen Y; Mao H; Yang KH; Abel T; Meaney DF A Modified Controlled Cortical Impact Technique to Model Mild Traumatic Brain Injury Mechanics in Mice. Front. Neurol 2014, 5, 100 DOI: 10.3389/fneur.2014.00100. [PubMed: 24994996]

(19). Pike BR; Flint J; Dutta S; Johnson E; Wang KKW; Hayes RL Accumulation of Non-Erythroid AII-Spectrin and Calpain-Cleaved AII-Spectrin Breakdown Products in Cerebrospinal Fluid after Traumatic Brain Injury in Rats. J. Neurochem 2001, 78, 1297–1306. DOI: 10.1046/j.1471-4159.2001.00510.x. [PubMed: 11579138]

(20). Saatman KE; Bozyczko-Coyne D; Marcy V; Siman R; McIntosh TK Prolonged Calpain-Mediated Spectrin Breakdown Occurs Regionally Following Experimental Brain Injury in the Rat. J. Neuropathol. Exp. Neurol 1996, 55, 850–860. DOI: 10.1097/00005072-199607000-00010. [PubMed: 8965100]

(21). Zhao X; Posmantur R; Kampfl A; Liu S-J; Wang KKW; Newcomb JK; Pike BR; Clifton GL; Hayes RL Subcellular Localization and Duration of μ-Calpain and m-Calpain Activity after Traumatic Brain Injury in the Rat: A Casein Zymography Study. J. Cereb. Blood Flow Metab 1998, 18, 161–167. DOI: 10.1097/00004647-199802000-00006. [PubMed: 9469158]

(22). Ringger NC; Tolentino PJ; McKinsey DM; Pike BR; Wang KKW; Hayes RL Effects of Injury Severity on Regional and Temporal MRNA Expression Levels of Calpains and Caspases after Traumatic Brain Injury in Rats. J. Neurotrauma 2004, 21, 829–841. DOI: 10.1089/0897715041526177. [PubMed: 15307896]

(23). Price L; Wilson C; Grant G Blood-Brain Barrier Pathophysiology Following Traumatic Brain Injury In Translational Research in Traumatic Brain Injury; Laskowitz D, Grant G, Eds.; CRC Press/Taylor and Francis Group: Boca Raton, FL, 2016; pp 85–96. DOI: 10.1201/b18959-5.

(24). Hicks RR; Baldwin SA; Scheff SW Serum Extravasation and Cytoskeletal Alterations Following Traumatic Brain Injury in Rats. Mol. Chem. Neuropathol 1997, 32, 1–16. DOI: 10.1007/BF02815164. [PubMed: 9437655]

(25). Kwon EJ; Skalak M; Lo Bu R; Bhatia SN Neuron-Targeted Nanoparticle for SiRNA Delivery to Traumatic Brain Injuries. ACS Nano 2016, 10, 7926–7933. DOI: 10.1021/acsnano.6b03858. [PubMed: 27429164]

(26). Caliceti P; Veronese FM Pharmacokinetic and Biodistribution Properties of Poly(Ethylene Glycol)-Protein Conjugates. Adv. Drug Deliv. Rev 2003, 55, 1261–1277. DOI: 10.1016/S0169-409X(03)00108-X. [PubMed: 14499706]

(27). Boyd BJ; Galle A; Daglas M; Rosenfeld JV; Medcalf R Traumatic Brain Injury Opens Blood-Brain Barrier to Stealth Liposomes via an Enhanced Permeability and Retention (EPR)-like Effect. J. Drug Target 2015, 23, 847–853. DOI: 10.3109/1061186X.2015.1034280. [PubMed: 26079716]

(28). Bharadwaj VN; Lifshitz J; Adelson PD; Kodibagkar VD; Stabenfeldt SE Temporal Assessment of Nanoparticle Accumulation after Experimental Brain Injury: Effect of Particle Size. Sci. Rep 2016, 6, 29988 DOI: 10.1038/srep29988. [PubMed: 27444615]

(29). Mitala CM; Wang Y; Borland LM; Jung M; Shand S; Watkins S; Weber SG; Michael AC Impact of Microdialysis Probes on Vasculature and Dopamine in the Rat Striatum: A Combined Fluorescence and Voltammetric Study. J. Neurosci. Methods 2008, 174, 177–185. DOI: 10.1016/j.jneumeth.2008.06.034. [PubMed: 18674561]

(30). Longmire M; Choyke PL; Kobayashi H Clearance Properties of Nano-Sized Particles and Molecules as Imaging Agents: Considerations and Caveats. Nanomedicine 2008, 3, 703–717. DOI: 10.2217/17435889.3.5.703. [PubMed: 18817471]

(31). Kwong GA; Dudani JS; Carrodeguas E; Mazumdar EV; Zekavat SM; Bhatia SN Mathematical Framework for Activity-Based Cancer Biomarkers. Proc. Natl. Acad. Sci. U. S. A 2015, 112, 12627–12632. DOI: 10.1073/pnas.1506925112. [PubMed: 26417077]

(32). Habgood MD; Bye N; Dziegielewska KM; Ek CJ; Lane MA; Potter A; Morganti-Kossmann C; Saunders NR Changes in Blood-Brain Barrier Permeability to Large and Small Molecules Following Traumatic Brain Injury in Mice. Eur. J. Neurosci 2007, 25, 231–238. DOI: 10.1111/j.1460-9568.2006.05275.x. [PubMed: 17241284]

(33). Stockholm D; Bartoli M; Sillon G; Bourg N; Davoust J; Richard I Imaging Calpain Protease Activity by Multiphoton FRET in Living Mice. J. Mol. Biol 2005, 346, 215–222. DOI: 10.1016/j.jmb.2004.11.039. [PubMed: 15663939]

(34). Levesque S; Wilson B; Gregoria V; Thorpe LB; Dallas S; Polikov VS; Hong JS; Block ML Reactive Microgliosis: Extracellular-Calpain and Microglia-Mediated Dopaminergic Neurotoxicity. Brain 2010, 133, 808–821. DOI: 10.1093/brain/awp333. [PubMed: 20123724]

(35). Thorek DLJ; Watson PA; Lee SG; Ku AT; Bournazos S; Braun K; Kim K; Sjostrom K; Doran MG; Lamminmaki U; et al. Internalization of Secreted Antigen-Targeted Antibodies by the Neonatal Fc Receptor for Precision Imaging of the Androgen Receptor Axis. Sci. Transl. Med 2016, 8, 367ra167 DOI: 10.1126/scitranslmed.aaf2335.

(36). Urano Y; Sakabe M; Kosaka N; Ogawa M; Mitsunaga M; Asanuma D; Kamiya M; Young MR; Nagano T; Choyke PL; et al. Rapid Cancer Detection by Topically Spraying a -Glutamyltranspeptidase-Activated Fluorescent Probe. Sci. Transl. Med 2011, 3, 110ra119 DOI: 10.1126/scitranslmed.3002823.

(37). Whitley MJ; Cardona DM; Lazarides AL; Spasojevic I; Ferrer JM; Cahill J; Lee C-L; Snuderl M; Blazer III DG; Hwang ES; et al. A Mouse-Human Phase 1 Co-Clinical Trial of a Protease-Activated Fluorescent Probe for Imaging Cancer. Sci. Transl. Med 2016, 8, 320ra4 DOI: 10.1126/scitranslmed.aad0293.

(38). Dudani JS; Ibrahim M; Kirkpatrick J; Warren AD; Bhatia SN Classification of Prostate Cancer Using a Protease Activity Nanosensor Library. Proc. Natl. Acad. Sci. U. S. A 2018, 115, 8954–8959. DOI: 10.1073/pnas.1805337115. [PubMed: 30126988]

(39). Guilfoyle MR; Carpenter KLH; Helmy A; Pickard JD; Menon DK; Hutchinson PJA Matrix Metalloproteinase Expression in Contusional Traumatic Brain Injury: A Paired Microdialysis Study. J. Neurotrauma 2015, 32, 1553–1559. DOI: 10.1089/neu.2014.3764. [PubMed: 25858502]

(40). Costa C; Tortosa R; Domènech A; Vidal E; Pumarola M; Bassols A Mapping of Aggrecan, Hyaluronic Acid, Heparan Sulphate Proteoglycans and Aquaporin 4 in the Central Nervous System of the Mouse. J. Chem. Neuroanat 2007, 33, 111–123. DOI: 10.1016/j.jchemneu.2007.01.006. [PubMed: 17349777]

(41). Mummert ME; Mohamadzadeh M; Mummert DI; Mizumoto N; Takashima A Development of a Peptide Inhibitor of Hyaluronan-Mediated Leukocyte Trafficking. J. Exp. Med 2000, 192, 769–779. DOI: 10.1084/jem.192.6.769. [PubMed: 10993908]

(42). Mann AP; Scodeller P; Hussain S; Joo J; Kwon E; Braun GB; Mölder T; She ZG; Kotamraju VR; Ranscht B; et al. A Peptide for Targeted, Systemic Delivery of Imaging and Therapeutic Compounds into Acute Brain Injuries. Nat. Commun 2016, 7, 11980 DOI: 10.1038/ncomms11980. [PubMed: 27351915]

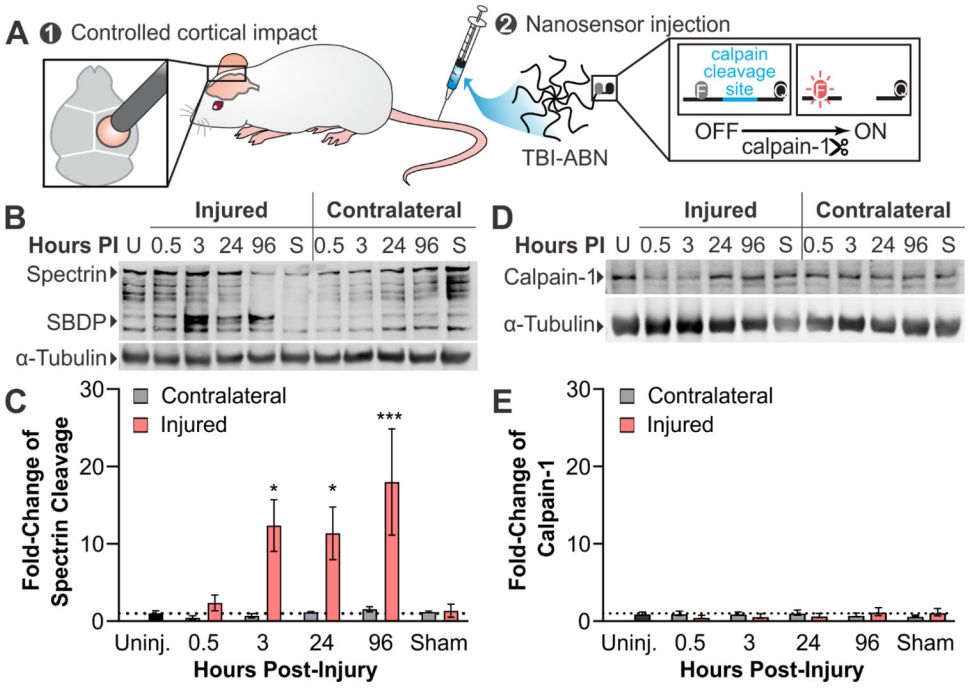

Figure 1.

Design of a TBI activity-based nanosensor. (A) Overview of TBI-ABN design. (B) Time course post-injury (PI) of αII-spectrin cleavage in CCI-injured cortices. (C) Quantification of calpain-1-specific 145 and 150 kDa αII-spectrin breakdown products (SBDP), normalized to α-tubulin and untreated control (n=3, mean ± SE, *p<0.05, ***p<0.001, two-way ANOVA and Dunnett's post-hoc test against uninjured control). (D) Time course and (E) quantification of 80 kDa calpain-1 denoted by the arrow normalized to α-tubulin and untreated control (n=3, mean ± SE). Uninjured (U) mice received no surgery. Sham (S) mice received a craniotomy and no injury.

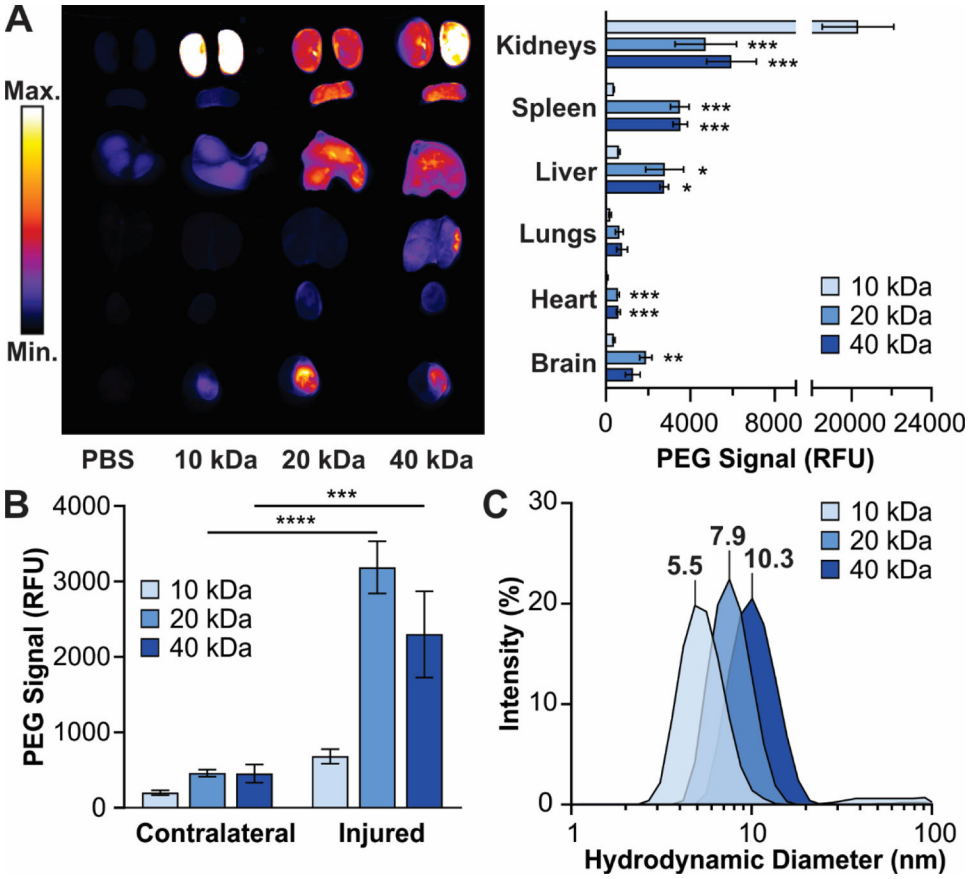

Figure 2.

Large molecular weight PEG carriers localize to the region of injury in a mouse model of TBI. (A) Fluorescence image of major organs after intravenous injection of fluorescently-labeled PEG of various sizes (left) were quantified and signal normalized to PBS injected animals (right) (n=4, mean ± SE, *p<0.05, **p<0.01, ****p<0.001, ordinary one-way ANOVA and Tukey's post-hoc test compared within each organ). (B) PEG distribution in injured or contralateral brain hemispheres (n=4, mean ± SE, ***p<0.001, ****p<0.0001, two-way ANOVA and Sidak's post-hoc test within each size). (C) Size distribution of 10 kDa, 20 kDa, and 40 kDa PEG.

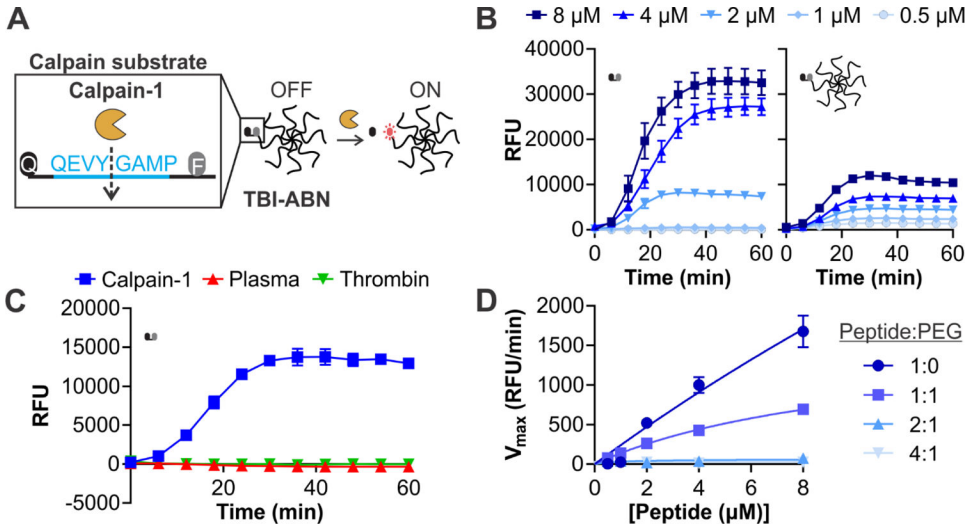

Figure 3.

Calpain substrate is cleaved by calpain-1 as free peptide and when conjugated to PEG carrier. (A) Schematic of calpain substrate peptide, conjugated to 8-arm PEG to form TBI-ABN (Q=quencher, F=fluorophore). (B) Cleavage of free peptide (left) and 1:1 peptide:PEG (right) with recombinant human calpain-1 (n=3, mean ± SD). (C) Cleavage of 8 μM peptide with recombinant human calpain-1, mouse plasma, or human alpha-thrombin (n=3, mean ± SD). (D) Michaelis-Menten reaction kinetics of peptide:PEG ratios of 1:0, 1:1, 2:1, and 4:1 calpain-1 cleavage (n=3, mean ± SD).

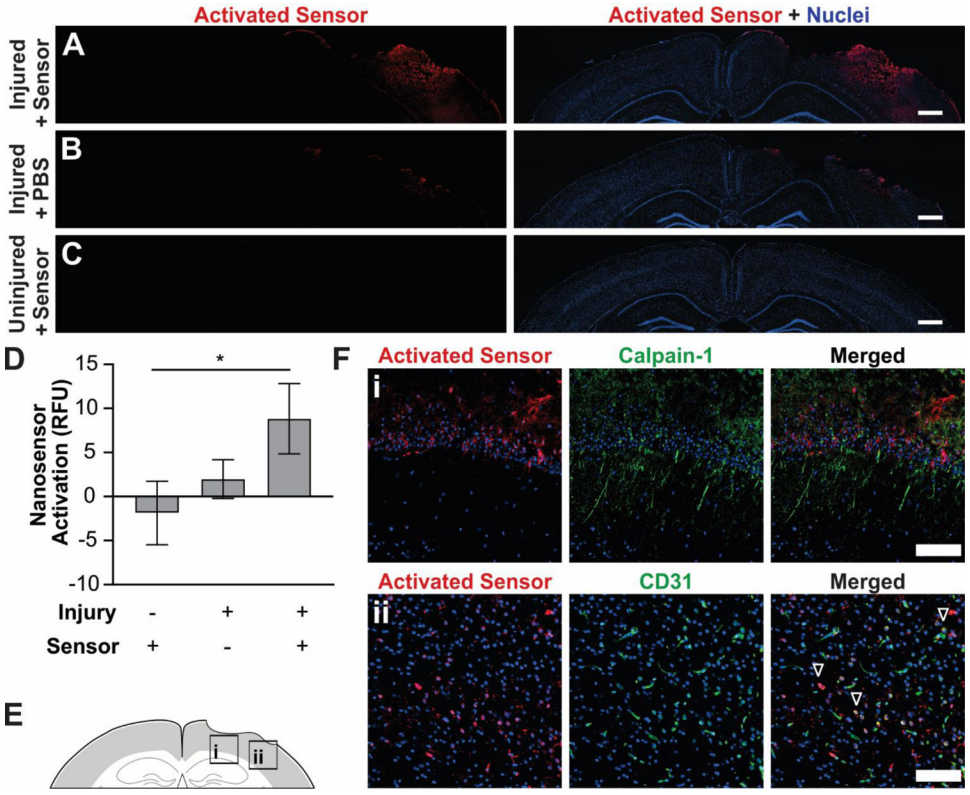

Figure 4.

Calpain sensor activates in injured brain tissue after intravenous delivery. (A-C) Representative coronal brain slices from injured and uninjured brains. (blue, nuclei; red, activated nanosensor; scale bar = 500 μm). (D) Quantification of mean sensor intensity in the injured hemisphere normalized to uninjured control brains (n=6, mean ± SE, *p=0.0851, ordinary one-way ANOVA and Sidak's post-hoc test). (E) Map and (F) insets from slices adjacent to Fig. 4A showing sensor localization relative to (i) calpain-1 and (ii) CD31 in the injury periphery (blue, nuclei; red, activated nanosensor; green, calpain-1 (top) or CD31 (bottom); outlined arrows, overlap of sensor with CD31; scale bar = 100 μm).